Brittle-ductile transition and associated seismicity: Experimental and numerical studies and relationship with the b-value

David Amitrano

Brittle-ductile transition and associated seismicity: Experimental and numerical studies and relationship with the b-value

David Amitrano

LAEGO, Ecole Nationale Supérieure des Mines de Nancy, France

Abstract. The acoustic emission (AE) and the mechanical behavior of granite samples during triaxial compression tests have been analyzed. The size of AE events displays power-law distributions, conforming to the Gutenberg-Richter law observed for earthquakes which is characterized by the b-value. As the confining pressure increases, the macroscopic behavior becomes more ductile. For all different stages of the rock mechanical behavior (linear, non-linear pre-peak, non linear post-peak, shearing), there is a systematic decrease of the b-value with increasing confining pressure. A numerical model based on progressive elastic damage and the finite element method allows simulations of the main experimental observations on AE and of a wide range of macroscopic behaviors from brittleness to ductility. The model reproduces a decrease in the b-value that appears to be related to the type of macroscopic behavior (brittle-ductile) rather than to the confining pressure. Both experimental and numerical results suggest a relationship between the b-value and the brittle-ductile transition. Moreover these results are consistent with recent earthquake observations and give new insight into the behavior of the Earth's crust.

1. Introduction

The mechanical loading of rocks involves local inelastic processes that produce acoustic wave emissions (AE). Nonlinearity of the macroscopic mechanical behavior results from these microscopic scale processes. For rocks loaded at high strain rate and low temperature, microfracturing is considered to be the main inelastic process [*Kranz*, 1983]. The correlation between AE activity and macroscopic inelastic strain has been established in many experimental [see *Lockner*, 1993, for a review] and numerical [e.g. *Young et al.*, 2000] studies.

As microfracturing progresses, cooperative interactions of cracks take place and lead to the coalescence of a macroscopic fracture, i.e. to the macrorupture [*Costin*, 1983; *Kranz*, 1983; *Reches and Lockner*, 1994; *Schulson et al.*, 1999]. This behavior has been experimentally observed by AE source location [*Lockner et al.*, 1991].

The macroscopic behavior of rocks ranges from brittleness to ductility depending on rock type and loading conditions (i.e. strain rate, confining pressure and temperature). Many definitions of brittle-ductile behavior based on the type of macroscopic behavior have been proposed [*Jaeger and Cook*, 1979]. The most simple is based on the amount of inelastic deformation before the macrorupture (Figure 1). A purely brittle material fails without any inelastic strain before the failure. By contrast, a purely ductile material strains without loss of strength. The failure, if any, occurs after a considerable amount of inelastic strain.

Paper number .
0148-0227/02/$9.00

Fracturing dynamics during mechanical loading, which can be studied through AE monitoring, usually displays a power law distribution of acoustic events size.

$$N(>A) = c.A^{-b} \tag{1}$$

Where A is the maximum amplitude of AE events, $N(>A)$ is the number of events with maximum amplitude greater than A, and c and b are constants. In a log-log representation, this distribution appears linear and b is given by the slope of the line.

$$logN(>A) = C - b.logA \tag{2}$$

This distribution exhibits remarkable similarity to the Gutenberg-Richter relationship observed for earthquakes [*Gutenberg and Richter*, 1954].

$$logN(>M) = a - bM \tag{3}$$

Where $N(>M)$ is the number of earthquakes with a magnitude larger than M.
Assuming that the magnitude is proportional to the log of the maximal amplitude of the seismic signal, the b-value obtained from the magnitude or the amplitude can be compared [*Weiss*, 1997]. Rigorously, the amplitude measured at a given distance from the source should be corrected for the attenuation. Nevertheless, theoretical [*Weiss*, 1997] and experimental studies [*Lockner*, 1993] have shown that attenuation has no significant effect on the b-value.

As power laws indicate scale invariance and because of the similarities in the physics of the phenomena (wave propagation induced by fast source motion), AE of rock observed in

the laboratory has been considered as a small-scale model for the seismicity in rock masses (rockbursts) or in the Earth's crust (earthquakes) [*Scholz*, 1968]. Observations of both earthquakes and AE show variations of the b-value in time and space domains which are usually explained using fracture mechanics theory and/or the self-organized criticality (SOC) concept. *Mogi* [1962] suggested that the b-value depends on material heterogeneity, a low heterogeneity leading to a low b-value. *Scholz* [1968] observed that the b-value decreases before the maximum peak stress is achieved and argued for a negative correlation between b-value and stress. *Main et al.* [1989] observed the same variation but invoked a negative correlation between the b-value and the stress intensity factor K. Following this idea, *Main et al.* [1989] proposed different patterns of b-value variation before macrorupture, driven by the fracture mechanics and the type of rupture (brittle-ductile). The relationship between the b-value and the fractal dimension D of AE source locations was also investigated [*Lockner and Byerlee*, 1991] and showed a decrease of b-value contemporary to the strain localization, i.e. to a decrease of D-value.

Mori and Abercombie [1997] observed a decrease of the b-value with increasing depth for earthquakes in California. They suggested that the b-decrease was related to a diminution of the heterogeneity as depth increases. Systematic tests of the dependence of the b-value on depth have been recently performed by *Gerstenberg et al.* [2001] which confirm these results. The depth dependence of the b-value have also been observed for the western Alps seismicity [*Sue et al.*, 2002] and for earthquakes sequence along the Aswan Lake in Egypt [*Mekkawi et al.*, 2002].

Other authors have used cellular automata [*Chen et al.*, 1991; *Olami et al.*, 1992] or lattice solid models [*Zapperi et al.*, 1997] to simulate power-law distribution of avalanches which appear to be associated with a ductile macroscopic behavior. Numerical models based on elastic damage [*Tang*, 1997; *Tang and Kaiser*, 1998] succeed in simulating brittle behavior. Discrete element models simulating macroscopic behavior ranging from brittle to ductile and power-law distributions of earthquakes have also been proposed [*Wang et al.*, 2000; *Li et al.*, 2000; *Place and Mora*, 2000]. *Wang et al.* [2000] argue that the b-value depends on the cracks density distribution but do not report a relation between the b-value and the type of mechanical behavior. *Amitrano et al.* [1999] proposed a model which simulates both ductile and brittle behavior and show that the b-value depends on the macroscopic behavior .

These results suggest that a relationship between the b-value and the macroscopic behavior may exist. The present paper reports results on AE monitoring of granite samples during triaxial compression tests and numerical simulations. We study the effect of the confining pressure on both the macroscopic behavior and the b-value.

2. Experimental procedure

2.1. Tested Rock

A set of 34 triaxial compression tests were performed on Sidobre granite. This rock contains 71% feldspar, 24.5% quartz, 4% mica and 0.5% chlorite. The grain sizes are in the range 1-2 mm for the feldspar, 0.5-1 mm for the quartz and 0.5-2 mm for the mica [*Isnard*, 1982]. The density is 2.65 and the continuity index obtained by sound velocity measurement (sonic velocity measured on the sample divided by the theoretical value for the intact rock) is about 97%. The sound velocity is about 4 800 m/s. The mean uniaxial compressive strength is 160 MPa, Young's modulus is 60 GPa and the Poisson's ratio is 0.24. The samples were 40 mm in diameter and 80 mm in length.

2.2. Experimental device

A hydraulic press of 3000 kN capacity was used. The confining pressure was applied by means of a triaxial cell. The stiffness of the complete loading system (press, piston, sample support) is about 10^9 N/m. The axial displacement of the platens was measured by an LVDT sensor. The sample strain was estimated from the displacement, taking into account the stiffness of the loading system (shortening of the piston and the sample support) and the length of the sample. The axial displacement rate was kept constant near 1 μm/s except during the macrorupture when dynamic failure occurs. A resonant transducer (Physical Acoustic Corporation,peak frequency : 135 kHz effective range frequency : 100 kHz - 1 MHz) was applied on the outside part of the cell piston which was used as a wave guide. The transducer was connected to a 40 dB preamplifier (PAC 1220A) with adapted filters (20 kHz-1.2 MHz) and then to an AE analyzer (Dunegan-Endevo 3000 Series) with 40 dB amplification which performed the AE counting. In parallel the signals were digitalized after preamplification by means of a fast acquisition board (Imtec T2M50, 8 bits). The sampling frequency was 5 MHz and the length of the recorded signals was 2048 samples, which corresponds to a duration of 410 μs. The signal recording trigger was set to 15 mV and the maximal amplitude to 1 V. The board memory segmentation allowed us to record several hundred signals per second without dead time.

2.3. Deformation mode

The Sidobre granite samples were deformed under varying conditions of confining pressure, ranging from 0 to 80 MPa. The axial displacement was applied at a constant strain rate except during the macrofailure which is unstable. Loading was continued after failure until the displacement along the macrorupture surface reached several millimeters.

2.4. Data processing

The AE counting was directly obtained from the analyzer. This parameter appeared to be well correlated with the AE energy calculated from the digitalized signals. The slope of the cumulative AE counting curve represents the AE activity. The digitalized signals were processed to extract the maximal amplitude and the energy for each signal.

The b-value was obtained from the inverse cumulative distribution of the events maximal amplitude. This distribution was fitted in a least square sense by a linear function in a log-log diagram. The slope of this curve gave the b-value. The error of estimation of the b-value has been calculated for a confidence level of 95%. The b-value was first calculated for all recorded events during each test. In order to observe variations of the b-value during the different stages of each test, the b-value was also calculated separately for events occurring during each stage of the mechanical behavior. The minimum number of events that was used for calculating the b-value was fixed at 200; according to *Pickering et al.* [1995] this population size is acceptable to calculate the b-value with a good accuracy, i.e. with standard deviation less than 0.1 for the b-value.

3. Experimental results

3.1. Mechanical behavior

A set of 34 tests have been performed with confining pressure ranging from 0 to 80 MPa. Figure 2 shows typical results obtained for a confining pressure of 60 MPa. We identify four stages in the mechanical behavior, as observed on the $\sigma(\epsilon)$ curve, and the acoustic emission activity.

• Stage 1 is defined by the first linear part of the $\sigma(\epsilon)$ curve. The initial part of this stage is influenced by the closing of microcracks as indicated by the increase in the slope of the stress-strain curve. After that, the mechanical behavior is linear and is not affected by microcracks. The AE activity is very low and can be attributed to the closure or shearing of prexisting cracks [*Lockner and Byerlee*, 1991]. The b-value is maximum.

• Stage 2 begins with the appearance of a non-linear behavior. It corresponds to a strain hardening stage as the strength increases with rock deformation. AE is caused by cracks propagation that affects the macroscopic behavior. The AE activity increases drastically by the end of stage 2 and the b-value decreases (figure 6).

• Stage 3 corresponds to the post-peak behavior preceding the macro-rupture. The rocks display strain softening, as the strength decreases with increasing strain. AE is produced by the propagation and coalescence of cracks. AE activity reaches its maximum value and the b-value is minimum. This stage ends with the macro-failure which is unstable. As addressed earlier by *Wawersick and Fairhurst* [1970], this instability occurs when the sample strength decreases with strain faster than the apparatus unloads. The starting and ending point of the unstable failure are strongly machine-dependent and are not relevant to the description of the rock sample behavior. It is generally assumed that the nucleation of a macroscopic discontinuity occurs simultaneously with the unstable failure.

• Stage 4 corresponds to the macrorupture surface shearing. AE is caused by the rupture of surface asperities and by gouge fracturing. The shear strength is nearly constant or slowly decreases and the AE rate slowly decreases .

3.2. Brittle-ductile transition

For each test we calculated $\sigma_1 - \sigma_3$ and ϵ_1 at the end of each stage. Figures 3 and 4 display these results for all of the tests. Stress and strain are plotted as functions of the confining pressure.

In order to estimate the brittle-ductile character of the mechanical behavior, we quantified the range of the inelastic behavior before macrorupture using two parameters. One is representing the inelastic strain, $\epsilon_{in.}$, and the second the stress range of stage 2, $\Delta\sigma_{in.}$. $\Delta\sigma_{in.}$ is the difference between the stress at the end of stage 1 and the peak stress (end of stage 2). This parameter quantifies the stress amplitude of the strain hardening stage. Inelastic strain, $\epsilon_{in.}$, is obtained by subtracting the elastic strain, $\epsilon_{el.}$, to the total strain,$\epsilon_{tot.}$, which is currently measured :

$$\epsilon_{in.} = \epsilon_{tot} - \epsilon_{el.} \tag{4}$$

The elastic strain is calculated using the elastic modulus estimated in the linear stage (dotted line in figure 2) and the current value of $\sigma_1 - \sigma_3$.

$$\epsilon_{el.} = E_{initial}.(\sigma_1 - \sigma_3) \tag{5}$$

Figure 5 presents the mean values of the differential stress, $\sigma_1 - \sigma_3$, and the axial strain, ϵ_1, as a function of the confining pressure. $\Delta\sigma_{in.}$ and $\epsilon_{in.}$ are also plotted. Since the starting and ending points of the unstable failure are strongly machine-dependent, we restrict the discussion to the values measured at the end of the linear stage 1 and at the peak (end of the stage 2).

For $\sigma_3 = 0$, which corresponds to an uniaxial compression test, the sample failed immediately after stage 1. The inelastic behavior range (i.e. $\Delta\sigma_{in.}$ and $\epsilon_{in.}$) is nearly zero; that corresponds to a purely brittle behavior. As the confining pressure increases, the stress levels for each stage increase at different rates. In particular the peak stress increases faster than the stress at the end of the linear stage, which indicates an increase in strain hardening. In the same manner, the amount of inelastic strain before the peak increases with the confining pressure. Hence, the range of inelastic behavior (i.e. $\Delta\sigma_{in.}$ and $\epsilon_{in.}$) increases with increasing confining pressure. This indicates that the pre-peak behavior becomes progressively more ductile. The range of confining pressure that we tested does not cover the entire brittle-ductile transition. Nevertheless, the analysis of the brittle-ductile characteristic which was performed on granite, a rock commonly considered as brittle, shows that even this material becomes increasingly ductile at relatively low confining pressure (the maximum confining pressure of 80 MPa corresponds to a 3.2 km depth for a natural geostatic stress field). Similar results were obtained by *Brace et al.* [1966] on granite for larger confining pressure range. They observed an increase in the range of inelastic behavior, before the peak, for sample triaxially loaded with confining pressure ranging from 0 to 800 MPa. However, as often observed for granite, the effect of the confining pressure on the behavior remains minor as the loading ever leads to an unstable failure.

3.3. b-value pressure dependence

In order to examine the relationship between the b-value and the confining pressure, we calculated the b-value for all AE events detected during each stage of each one of the tests. Figure 6a displays the cumulative distributions of AE amplitude for a representative test performed at $\sigma_3 = 60MPa$, showing separately the events recorded during each mechanical stage. As classically observed, the b-value is maximal during stage 1, then decreases during stage 2 and reaches its minimal value during stage 3.

Figure 6b displays the AE amplitude distributions for a set of 4 tests at confining pressures ranging from 0 to 80 MPa. Each distribution includes all of the events recorded during the test. The b-value decreases with increasing confining pressure.

Figure 7 displays the b-value corresponding to the different stages of mechanical behavior for all of the tests, as a function of σ_3. Figure 8 presents the mean b-values for each stage as a function of the confining pressure (a) and of the differential stress (b). The b-value is negatively correlated with both the confining pressure and with the differential stress. This behavior is observed for each of the stages as well as for the b-values calculated for the entire test (i.e. without grouping the recorded events according to the stages).

For each stage, the b-value, appears to decrease linearly with increasing differential stress. The decreasing rate varies from one stage to the other: the highest rate is observed for stage 1. Stages 2 and 3 reveal very similar trends and the smallest effect of the differential stress. Stage 4 is an intermediate case. By contrast, the relationship between the b-value and confining pressure shows approximately the same decreasing rate for all of the stages. One may note that the differential stress and the confining pressure are not independent parameters, and that their relationships depend on the mechanical stage (figure 5a). The relationship between the b-value and the confining pressure appears to be more general, as the same behavior is observed for all the stages of mechanical behavior. Therefore, the confining pressure appears as a more relevant parameter than the differential stress for describing variation in b-value. As far as we know, this effect of the confining pressure on the b-value has never been experimentally demonstrated before. These observations are consistent with numerical results obtained by *Amitrano et al.* [1999].

The next section presents further numerical simulations of these laboratory experiments.

4. Numerical simulation

The model proposed by *Amitrano et al.* [1999] simulates a wide range of mechanical behaviors from ductility to brittleness, and shows that the simulated b-value and the macroscopic behavior of the model are related. For the present work, we use this model for simulating both the mechanical behavior and acoustic emission observed during laboratory tests, and particularly the relationship between the b-value and the brittle-ductile transition induced by the increase in confining pressure.

4.1. Numerical model features

The model proposed by *Amitrano et al.* [1999] is based on a progressive isotropic damage that is represented by the reduction of the elastic modulus. The effective elastic modulus, $E_{eff.}$, is expressed as a function of the initial modulus, $E_{ini.}$, and the damage parameter, D.

$$E_{eff.} = (1 - D).E_{ini.} \tag{6}$$

Such a relationship is valid for a domain which is large as compared with the defect size. In such a case, the damage can be parameterized by crack density [*Kemeny and Cook*, 1986]. The simulated material is discretized using a finite element method with plane-strain hypothesis. The element scale is considered as a meso-scale, i.e. intermediate between the micro-scale corresponding to defects and the macro-scale corresponding to the whole model. The loading consists of increasing the vertical displacement of the upper model boundary. After each loading step, when the stress of an element exceeds a given strength threshold for damage, its elastic modulus is multiplied by a factor $(1 - D)$, D being a constant. Because of the elastic interaction, the stress redistribution around a damaged element can induce damage on adjacent elements and lead to an avalanche of damaged elements. The avalanche size corresponds to the total number of damaged elements during a single loading step. This size is comparable to the AE activity induced by stress change [*Meredith et al.*, 1990]. In the original version of the model the damage threshold was based on the Mohr-Coulomb criterion.

$$\tau = C + \sigma tan\phi \tag{7}$$

where τ is the shear stress; σ is the normal stress; C is the cohesion; and ϕ is the internal friction angle. In order to simulate material heterogeneity, the value of the cohesion C is randomly drawn from a uniform distribution. This feature is necessary to obtain macroscopic behaviours differing from those of the elements and a power law distribution of the events size. The Mohr-Coulomb criterion allows us to consider separately the effect of cohesion, internal friction angle and confining pressure. The sensitivity studies performed by *Amitrano et al.* [1999] showed that both the b-value and the type of mechanical behavior (brittle/ductile) remained unchanged when changing the cohesion or the confining pressure. On the contrary, changing the internal friction angle modified drastically both the b-value and the macroscopic mechanical behavior. Hence, the key parameter in this model is the internal friction angle, ϕ, which allows us to switch from ductility ($\phi \leq 20°$) to brittleness ($\phi \geq 40°$). Figure 9 shows simulation results for $tan\phi$ ranging from 0 to 1 (ϕ varying from 0 to 45°). The b-value for these simulations ranges from 0.63 to 1.2 as the simulated behavior varies from ductile to brittle. The internal friction angle also influences the final damage distribution which varies from diffuse to localized when ϕ increases. Note that in all cases, the damage events are diffuse in all the sample at the beginning of the simulation. For the brittle cases, the damage localization occurs suddenly during the macrofailure. For the intermediate cases, the localization occurs progressively during the post-peak. For the ductile case the damage distribution stays diffuse during all the simulation.

The Mohr-Coulomb criterion does not reflect the fact that the internal friction angle decreases as the confining pressure increases, which is usually observed during laboratory experiments [see *Savage et al.*, 1996, for a discussion]. A non-linear criterion is required for taking into account this pressure dependence of the internal friction angle. Here we choose to use the empirical criterion proposed by *Hoek and Brown* [1982], which is considered to be relevant for a wide range of rock types.

$$\sigma_1 = \sigma_3 + \sigma_c \sqrt{m \frac{\sigma_3}{\sigma_c} + 1} \tag{8}$$

where σ_c is the uniaxial compressive strength and m is an empirical parameter controling the pressure dependence of the criterion slope. A low value of m corresponds to a faster decrease of the slope with increased confining pressure. The m parameter appears to be empirically related to the brittle/ductile behavior. A high m value corresponds to a highly brittle behavior (see *Hoek and Brown* [1982] for a further discussion on the significance of this parameter).

4.2. Simulation of the Sidobre granite behavior

The Hoek and Brown criterion was evaluated for stress peak values observed in the laboratory (figure 10), in order to simulate the behavior of the Sidobre granite. The parameters corresponding to our laboratory results are $\sigma_c =$ 165 MPa and $m = 22$. These two parameters are used as

input for the numerical simulations. Simulations are performed for confining pressure ranging from 0 to 100 MPa.

Typical mechanical and seismic behaviors obtained from a simulation performed for σ_3=60 MPa are presented in figure 11. One may observe that macroscopic non-linear behavior is associated with the onset of seismic activity. The seismic activity increases until the macrorupture occurs and then decreases during the shearing stage. This behavior displays remarkable similarity with the one observed during our laboratory tests (figure 2) and by other authors [e.g. *Brace et al.*, 1966]. The major difference with laboratory tests is that the simulated macrorupture occurs without any macroscopic strain increase. This is due to the fact that the loading system we simulated has an infinite stiffness. Hence, there is no elastic energy released by the loading system to the sample.

Mechanical behaviors obtained from simulations performed for different values of the confining pressure are presented in figure 12. As the confining pressure increases both the strength and the inelastic range before failure increase. This is in agreement with the laboratory observations (figure 5).

In order to quantify the brittle-ductile behavior characteristics, values of $\Delta\sigma_{in.}$ and $\epsilon_{in.}$ (defined in the preceding section) are calculated. These parameters are presented in figure 13. The inelastic range increases with the confining pressure in accordance with the laboratory observations. This indicates that the macroscopic behavior changes from brittle to more ductile, but without covering the entire brittle-ductile transition. This is due to the fact that the simulated material, which is granite, is still brittle at confining pressures lower than 100 MPa.

4.3. Simulation of the Brittle-Ductile transition

This section presents simulations of the behavior of more ductile materials for which the complete brittle-ductile transition can be covered within the same range of confining pressure as considered above for granite. We simulated the behavior of materials for which the complete transition is observable under usual laboratory conditions (i.e. confining pressure lesser than 100 MPa): Darley-Dale sandstone and Carrara marble respectively. The parameters of the Hoek and Brown criterion corresponding to these materials are given in table 1.

The simulated macroscopic behaviors for these materials are presented on figure 14. For both materials, the simulated macroscopic behavior changes from brittle to ductile as the confining pressure increases. This is usually observed in laboratory [*Jaeger and Cook*, 1979; *Scholz*, 1990; *Hoek and Brown*, 1982].

Figure 15 presents the b-value as a function of the confining pressure for each simulated material. For both sandstone and marble, the b-value decreases as the confining pressure increases for low confining pressure. It stabilizes to a value near 1 for higher confining pressures for which the behavior becomes completely ductile ($\sigma_3 > 60$ MPa for the marble, $\sigma_3 > 80$ MPa for the sandstone). We recall that in the case of granite, for which the behavior never becomes purely ductile, the b-value decreases continuously and does not reach a minimum. These simulation results suggest that the b-value is related to the type of macroscopic behavior (brittle/ductile) rather than to the confining pressure.

4.4. b-value and damage localization

As displayed on figure 9, the macroscopic behavior (brittle/ductile) is related to the type of spatial distribution of the damage (localized/diffused). This is in remarkable agreement with the classical observations that distributed deformation is associated with ductility whereas localized deformation is associated to brittleness. In order to quantitatively estimate the damage localization, we calculated the spatial correlation dimension of damage, D, using the correlation integral method proposed by *Grassberger and Prococcia* [1983]. The spatial correlation integral is defined as :

$$C(r) = \frac{2}{N(N-1)} N(R > r) \tag{9}$$

where N is the total number of damage events, $N(R > r)$ is the number of pairs of events separated by a distance smaller than r. If this integral exhibits a power-law, $C(r) \sim r^D$, the population can be considered as fractal and D is the fractal dimension. In order to estimate the width of the power law behavior, we used the two-points slope technique. The local curve slope, s_l, is calculated between every point of the integral ($s_l = \Delta C(r)/\Delta r$). The range over which s_l is constant, gives the width of the power-law behavior. For this range, $C(r)$ is fitted in a least square sense by a linear function in a log-log diagram. The slope gives the D-value. We calculated both b and D values for 75 simulations for different values of σ_c and m parameters. The results are plotted on the figure 16. The b and D values appear to be negatively correlated. This indicates that diffused damage is associated with low b-value, whereas localized damage is associated with high b-value.

5. Discussion

5.1. Brittle-ductile transition as driven by the internal friction angle

Experimental results have shown that the macroscopic behavior of granite becomes more ductile as the confining pressure increases, even if this change is limited. This change of macroscopic behavior has been quantitatively estimated through the amount of inelastic strain before the peak. This is a usual result which has been previously observed by many authors on different rock types [e.g. *Jaeger and Cook*, 1979; *Hoek and Brown*, 1982; *Kranz*, 1983; *Savage et al.*, 1996; *Escartin et al.*, 1997]. This change of macroscopic behavior is related to a decrease of the internal friction angle. Because of the correlation between the confining pressure and the internal friction existing for natural materials it is difficult to separate experimentally the effect of these two parameters on the brittle-ductile transition.

Using a damage based model, *Amitrano et al.* [1999] investigated separately the effect of the confining pressure, the cohesion and the internal friction angle, using the Mohr-Coulomb criterion. These results show that the macroscopic behavior depends only on the internal friction angle and not on the confining pressure nor on the cohesion. Figure 9 shows that the type of macroscopic behavior ranges from ductility to brittleness for ϕ value ranging from 0 to 45°. This transition is associated with a change on the damage localization mode which varies from diffuse to localized. These numerical results are in good agreement with usual laboratory observations.

According to simulations performed with the Mohr-Coulomb criterion, the behavior does not depend on the confining pressure [*Amitrano et al.*, 1999], which is not in agreement with laboratory observations. This discrepancy can be attributed to the fact that the criterion slope (i.e. the internal friction angle) is not pressure dependent. Using a non-linear criterion for which the slope is pressure dependent [*Hoek and Brown*, 1982], we were able to simulate the change of mechanical behavior as the confining pressure increases. For this criterion, the m parameter controls the rate of slope decrease, as the confining pressure increases. This parameter has been proposed by *Hoek and Brown* [1982] to be an indicator of the brittleness of the behavior, i.e. a high m value corresponds to a highly brittle behavior. Simulations performed with different values of m corresponding to different rock types (granite, sandstone, marble) show that the brittle-ductile transition is obtained at a lower confining pressure as m is lower. This is in agreement with the investigation of *Hoek and Brown* [1982] on the brittle-ductile transition.

Based on these results, we argue that the key factor for the brittle-ductile transition is the internal friction angle rather than the confining pressure.

However, we stress that the empirical decrease of internal friction with increased confining pressure, which is observed for all of the rock types we studied (granite, marble, sandstone), reflects physical processes that are fundamentally different. For the granite, as for other crystalline rocks, it has been shown that increased confining pressure leads to a change in micro-fracturing processes [*Escartin et al.*, 1997; *Velde et al.*, 1993; *Jaeger and Cook*, 1979]. At low confining pressure, the dominant process is tensile cracks (mode I) parallel to the main stress direction. As the confining pressure increases, tensile cracks are progressively replaced by shear cracks (mode II-III). This change on the micro-scale processes is associated with a decrease of the internal friction, as mode II-III cracks are less pressure sensitive than mode I cracks.

For porous rocks like sandstone, brittle-ductile transition is associated with the transition from dilating shear bands to compacting shear bands [*Menendez et al.*, 1996; *Besuelle*, 2001]. As the confining pressure increases, intergranular cracking is progressively replaced by crushing and pore collapse. The effect of confining pressure is to impede dilatant deformation which is replaced by a non-dilatant one.

For rocks constituted by more ductile minerals, at room temperature, or when the temperature is high, one must consider the competition between cracking and crystal plasticity. On one hand, crack propagation occurs when the tensile strength at the crack tips is reached. The increase of confining pressure tends to close the cracks and impedes their propagation. On the other hand, dislocation glide, involved in mineral plasticity, depends only on the applied shear stress, and consequently is relatively insensitive to the confining pressure. Hence, as the confining pressure increases, crack propagation is progressively replaced by plasticity. This has been experimentally observed for Carrara marble at room temperature [e.g. *Fredrich et al.*, 1989], as for quartz and olivine at higher temperature [e.g. *Darot et al.*, 1985; *Hirth and Tullis*, 1992b, a].

All these observations show the diversity of the micro-scale processes involved in the brittle-ductile transition. However, they all show a decrease of the internal friction angle as the confining pressure increases. The variations of such a parameter capture a wide range of processes. Hence, it appears as a relevant parameter for the model we used, as this model neglects the detail of low scale micromechanisms and considers the element at meso-scale.

One remaining question is how the internal friction acts in the model to control both the macroscopic behavior, the damage localization and the b-value. In a previous study, *Amitrano* [1999] investigated the influence of the internal friction angle on the geometry of interaction between defects. The authors studied the field of the Mohr-Coulomb criterion (so-called F) around isolated defects (i.e. damaged zone). This field indicates the distance between the stress state and the failure criterion. The internal friction angle appeared to strongly influence the anisotropy of the F field around the defect. Low friction leads to a quasi-isotropic field whereas high friction leads to a highly anisotropic field. Hence, a low ϕ value allows interaction with other defects in any direction (diffuse interaction). A high value of ϕ induces a strong directionality restricting the possible interaction domain (localized interaction). At the macroscopic scale, this local interaction leads to a damage distribution which varies form diffuse to localized, depending on the ϕ value.

For what concerns the impact on the macroscopic behavior, we observed that, for brittle behavior, the macrofailure (near instantaneous major stress decrease) of the simulated sample was associated with a sudden localization of the damage. Hence, the elastic energy contained in all the sample is released into a localized area which leads to a huge damage event and consequently to a significant stress decrease. On the other hand, for a ductile behavior, the damage localization, if any, occurred progressively, in the absence of stress decrease. Hence, we suggest that this kind of macroscopic behavior results from the damage localization mode, which is controlled by the internal friction angle.

For what concerns the relationship between the friction angle and the b-value, we can propose the following explanation, which is also based on the interaction geometry. We have seen previously that the isotropy/anisotropy of the damage criterion (F) determines the geometrical interaction between defects. For an isotropic field, when a damage event occurs into an element, it can induce damage in all the surrounding elements. This facilitates the emergence of large events, which corresponds to a low b-value. On the other hand, an anisotropic field allows interaction preferentially in the direction of anisotropy. This restricts the emergence of large events, which corresponds to a high b-value. This qualitative explanation is confirmed by the quantitative results presented in figure 16, where the damage localization is estimated by the D-value.

5.2. Brittle-ductile transition, b-value and earth crust behavior

Experimental results show that the rock behavior becomes more ductile as the confining pressure increases. We also observe a systematic decrease of the b-value as the confining pressure increases. This suggests that a relationship may exist between the b-value, reflecting the damage dynamics at low scale, and the macroscopic behavior (brittle-ductile). The decrease of b-value with confining pressure is observed for different types of mechanical behavior and particularly for shear faulting, which is generally supposed to be the main mechanism for earthquakes [*Scholz*, 1990]. Therefore our results can give new insights into earthquakes

dynamics. In our experimental study, the confining pressure ranges from 0 to 80 MPa, which corresponds roughly to a natural stress state at depths ranging from 0 to 3200 m. These experimental results suggest that, in this range, the b-value variation with depth can reach 0.5.

Numerical simulations show that the b-value depends on the macroscopic behavior, which is controlled by the internal friction angle rather than by the confining pressure. Depending on the rock type, the decrease of the b-value is obtained at different confining pressures. The decrease of the b-value is obtained at lesser confining pressure for a ductile material than for a brittle one. Based on these results, we suggest that the b-value is related to the type of macroscopic behavior (brittle/ductile), rather than to confining pressure.

Both experimental and numerical results are in agreement with several earthquake observations. *Mori and Abercombie* [1997] observed a depth dependence of b-value for earthquakes of California between 1974 and 1996. Based on the study of *Mogi* [1962], they invoked the effect of heterogeneity, which they assumed to be decreasing with depth and could result in a reduced b-value. We suggest that such depth dependence of the b-value could also be due to an increase in confining pressure as depth increases. Our laboratory results are comparable to these observations but argue for a different explanation for the b-value decrease. In our experiments, the heterogeneity is constant and the only variable parameter is the confining pressure. Moreover, the numerical simulations show that the brittle-ductile transition is controlled by the decrease in the internal friction angle, induced by the pressure increase rather than by the confining pressure itself. We suggest that the b-value decrease is related to the change of mechanical behavior with depth, rather than to a change of heterogeneity nor to an increase of confining pressure.

Our results are also in agreement with *Gerstenberg et al.* [2001] who performed systematic tests of the dependence of the b-value on depth at California. They observed that, for more than 70% of the studied area, the b-value is significantly smaller in depth. According to these authors, the areas where depth dependence of the b-value is not observed correspond to zones where the geostress state shows anomalous variation with depth. Our results suggest that this could be related to a particular trend of the confining pressure with depth or to regional variations of the mechanical behavior of the crust, which can be more or less brittle or ductile. Recently, a statistical analysis of the western Alps seismicity between 1987-1999 highlighted significant difference in b-value observed for two seismic zones characterized by different earthquake depth distributions [*Sue et al.*, 2002]. The deeper one displays a lower b-value. Similar observations have been done for the 1982-1999 earthquakes sequence along the Aswan Lake in Egypt [*Mekkawi et al.*, 2002].

6. Conclusion

Experimental results shows two effects of the increase of confining pressure on the behavior of granite samples. On one hand the behavior becomes more ductile as the confining pressure increases. On the other hand, the b-value of acoustic emission size associated with different mechanical behavior decrease with the confining pressure. The numerical model we proposed is able to simulate the brittle-ductile transition as the confining pressure increases. Numerical results show that the b-value is controlled by variations of the internal friction angle induced by changes on the confining pressure.

Both experimental and numerical results are consistent with earthquake observations, which show a decrease in b-value with depth and give a new explanation for this decrease. The b-value decrease could result from the change from brittleness to ductility as the depth increases.

Acknowledgments. The author thanks Y.Orengo and D. Hantz for their technical support during the laboratory experiments; JR Grasso, F. Lahaie, A. Helmstetter and J. Weiss for helpful comments; A. Rouleau and H. Lopez for improvements of the manuscript; G. Hirth, N. Beeler and an anonymous reviewer whose critical remarks helped to improve this paper. This work was supported by the French program INSU-ACI CATNAT.

References

Amitrano, D., Emission acoustique des roches et endommagement: Approches experimentale et numrique, Application a la sismicite miniere, Phd thesis, Universite Joseph Fourier, 1999.

Amitrano, D., J.-R. Grasso, and D. Hantz, From diffuse to localized damage through elastic interaction, *Geophysical Research Letters*, *26*(14), 2109–2112, 1999.

Besuelle, P., Compacting and dilating shear bands in porous rock: Theoretical and experimental conditions., *Journal of Geophysical Research*, *106*(B7), 13435–13442, 2001.

Brace, W., B. Paulding, and C. Scholz, Dilatancy in the fracture of cristalline rocks, *Journal of Geophysical Research*, *71*(16), 3939–3953, 1966.

Chen, K., P. Bak, and S. Obukhov, Self-organized criticality in a crack-propagation model of earthquakes, *Physical Review A*, *43*(2), 625–630, 1991.

Costin, L., A microcrack model for the deformation and failure of brittle rock, *Journal of Geophysical Research*, *88*(B11), 9485–9492, 1983.

Darot, M., Y. Gueguen, and Z. Bencheman, Ductile-brittle transition investigated by micro-indentation : results for quartz and olivine, *Phys. Earth and Plan. Int.*, *40*, 180–186, 1985.

Escartin, J., G. Hirth, and B. Evans, Non dilatant brittle deformation of serpentinites: Implications for Mohr-Coulomb theory and the strength of faults, *Journal of Geophysical Research*, *102*(B2), 2897–2913, 1997.

Fredrich, J., B. Evans, and T. Wong, Micromechanics of the brittle to plastic transition in Carrara marble, *Journal of Geophysical Research*, *4129-4145*, 1989.

Gerstenberg, M., S. Wiemer, and D. Giardini, A systematic test of the hypothesis that b varies with depth in California, *Geophysical Research Letters*, *28*(1), 57–60, 2001.

Grassberger, P., and I. Prococcia, Measuring the strangeness of stange attractors, *Physica*, *9*, 189–208, 1983.

Gutenberg, B., and C. Richter, *Seismicity of the earth and associated phenomena*. Princeton University Press, Princeton, 2nd edition edn., 1954.

Hirth, G., and J. Tullis, The brittle-plastic transition in experimentally deformed quartz aggregates, *Journal of Geophysical Research*, *99*(B6), 11731–11747, 1992a.

Hirth, G., and J. Tullis, Dislocation creep regimes in quartz aggregates, *Journal of Structural Geology*, *14*(2), 145–159, 1992b.

Hoek, E., and E. Brown, *Underground excavations in rock*. Institution of Mining and Metallurgy, London, 1982.

Isnard, P., Etude chimique du massif granitique du Sidobre (Tarn), Technical report, Ecole National de Geologie, 1982.

Jaeger, J. C., and N. G. W. Cook, *Fundamentals of rock mechanics*. Chapman and Hall, London, 1979.

Kemeny, J., and N. G. W. Cook, Effective moduli, Non-linear deformation and strength of a cracked elastic solid, *Int. J. Rock Mech. Min. Sci. and Geomech. Abstr.*, *23*(2), 107–118, 1986.

Kranz, R., Microcracks in rocks: a review, *Tectonophysics*, *100*, 449–480, 1983.

Li, H., Y. Bai, M. Xia, M. Ke, and X. Yin, Damage localisation as a possible precursor of earthquake rupture, *Pageoph*, *157*, 1929–1943, 2000.

Lockner, D., The role of acoustic emission in the study of rock fracture, *Int. J. Rock Mech. Min. Sci. and Geomech. Abstr.*, *30*(7), 883–899, 1993.

Lockner, D., and J. Byerlee, Precursory AE patterns leading to rock fracture, in *Vth Conf. AE/MS Geol. Str. and Mat.*, edited by Hardy, pp. 45–58, The pennsylvania State University. Trans Tech Publication, Clausthal-Zellerfeld, Germany, 1991.

Lockner, D., J. Byerlee, V. Kuskenko, A. Ponomarev, and A. Sidorin, Quasi-static fault growth and shear fracture energy in granite, *Nature*, *350*, 39–42, 1991.

Main, I., P. Meredith, and C. Jones, A reinterpretation of the precursory seismic b-value anomaly from fracture mechanics, *Geophysical Journal*, *96*, 131–138, 1989.

Mekkawi, M., A. Hassoup, J. Grasso, and P. Schnegg, Fractal and spectral analysis of the earthquake sequences along the Aswan Lake, Egypt, in *26th General Assembly of the European Geophysical Society*, vol. Geophysical Research Abstracts, Volume 4, 2002, pp. abstract nEGS02–A–00027, Nice. 2002.

Menendez, B., W. Zhu, and T.-F. Wong, Micromechanics of brittle faulting and cataclastic flow in Berea Sandstone, *Journal of Structural Geology*, *18*(1), 1–16, 1996.

Meredith, P., I. Main, and C. Jones, Temporal variation in seismicity during quasi-static and dynamic failure, *Tectonophysics*, *175*, 249–268, 1990.

Mogi, K., Magnitude frequency relations for elastic shocks accompanying fractures of various materials and some related problems in earthquakes, *Bull. Earthquake Res. Inst. Univ. Tokyo*, *40*, 831–853, 1962.

Mori, J., and R. Abercombie, Depth dependence of earthquake frequency-magnitude distributions in California: Implication for rupture initiation, *Journal of Geophysical Research*, *102*(B7), 15081–15090, 1997.

Olami, Z., H. Feder, and K. Christensen, Self-organised criticality in a continuous, nonconservative cellular automaton modeling earthquake., *Physical Review Letters*, *68*(8), 1244–1247, 1992.

Pickering, G., J. Bull, and D. Sanderson, Sampling power-law distributions, *Tectonophysics*, *248*, 1–20, 1995.

Place, D., and P. Mora, Numerical simulation of Localisation phenomena in a fault zone, *Pageoph*, *157*, 1821–1845, 2000.

Reches, Z., and D. Lockner, Nucleation and growth of faults in brittle rocks, *Journal of Geophysical Research*, *99*(B9), 18159–18173, 1994.

Savage, J., J. Byerlee, and D. Lockner, Is internal friction friction, *Geophysical Research Letters*, *23*(5), 487–490, 1996.

Scholz, C. H., The frequency-magnitude relation of microfracturing in rock and its relation to earthquakes, *Bulletin of the Seismological Society of America*, *58*(1), 399–415, 1968.

Scholz, H., *The mechanics of earthquakes and faulting*. Cambridge University Press, 1990.

Schulson, E., D. Illiescu, and C. Renshaw, On the initiation of shear faults during brittle compressive failure: A new mechanism, *Journal of Geophysical Research*, *104*(B1), 695–705, 1999.

Sue, C., J. Grasso, F. Lahaie, and D. Amitrano, Mechanical behavior of western alpine structures inferred from statistical analysis of seismicity, *Geophysical Research Letters*, *29*(8), 65–1 65–4, 2002.

Tang, C., Numerical simulation of progressive rock failure and associated seismicity, *Int. J. Rock Mech. Min. Sci. and Geomech. Abstr.*, *34*(2), 249–261, 1997.

Tang, C., and P. Kaiser, Numerical simulation of cumulative damage and seismic energy release during brittle rock failure - Part I: Fundamentals, *Int. J. Rock Mech. Min. Sci. and Geomech. Abstr.*, *35*(2), 113–121, 1998.

Velde, B., D. Moore, A. Badri, and B. Ledesert, Fractal analysis of fractures during brittle to ductile changes, *Journal of Geophysical Research*, *98*(B7), 11935–11940, 1993.

Wang, Y., X. Yin, M. Ke, M. Xia, and K. Peng, Numerical simulation of rock failure and earthquake process on mesoscopic scale, *Pageoph*, *157*, 1905–1928, 2000.

Wawersick, W., and C. Fairhurst, A study of brittle rock fracture in laboratory compression experiments, *Int. J. Rock Mech. Min. Sci. and Geomech. Abstr.*, *7*, 561–575, 1970.

Weiss, J., The role of attenuation on acoustic emission amplitude distributions and b-values., *Bulletin of the Seismological Society of America*, *87*(5), 1362–1367, ns, 1997.

Young, R., J. Hazzard, and W. Pettitt, Seismic and micromechanical studies of rock fracture, *Geophysical Research Letters*, *27*(12), 1767–1770, 2000.

Zapperi, S., A. Vespignani, and E. Stanley, Plasticity and avalanche behaviour in microfracturing phenomena, *Nature*, *388*(14 august 1997), 658–660, 1997.

D. Amitrano, Laboratoire Environnement Géomécanique et Ouvrages, Ecole Nationale Supérieure des Mines de Nancy, Parc de Saurupt, 54042 Nancy Cedex, France.

(Received XX; revised XX;
accepted XX.)

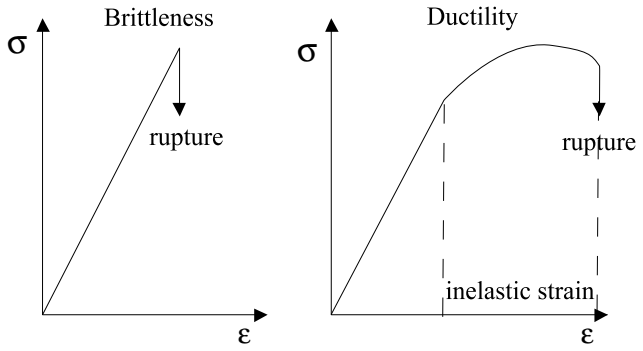

Figure 1. Brittleness and ductility as characterized by the stress-strain curve $\sigma(\epsilon)$. Brittleness is characterized by the absence of inelastic strain before failure. On the contrary ductility involves a considerable inelastic strain before failure.

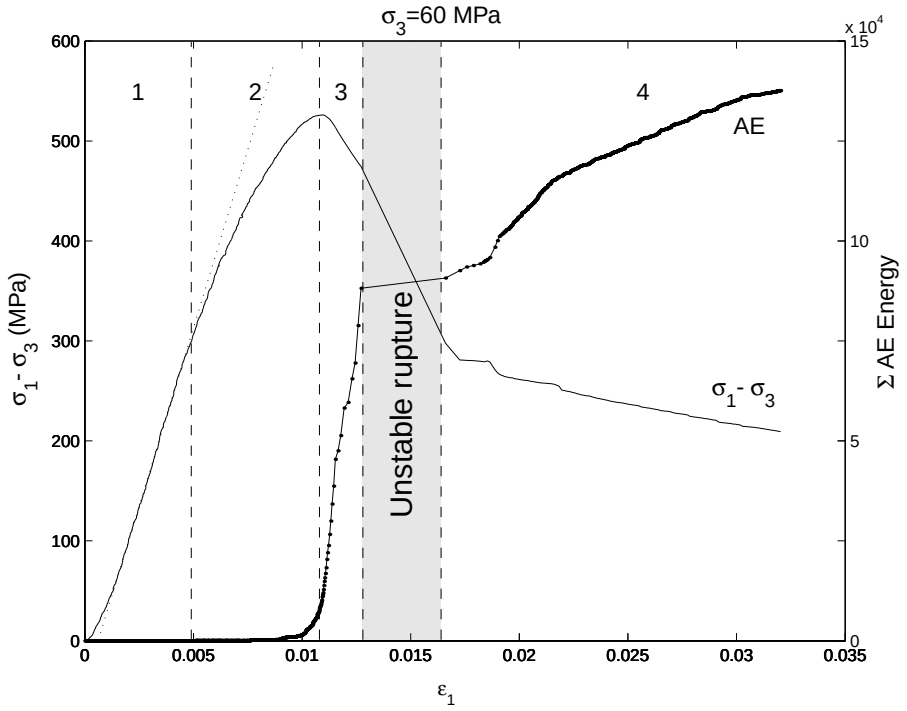

Figure 2. Typical mechanical behavior observed for triaxial compression tests. σ_1 is the longitudinal compressive stress, σ_3 the confining pressure, ϵ_1 the longitudinal strain. The differential stress, $\sigma_1 - \sigma_3$, and the cumulative acoustic emission energy, ΣAE_{Energy}, are plotted as functions of ϵ_1. Stage 1 corresponds to the initial linear behavior, stage 2, to the non-linear pre-peak behavior, stage 3, to the post-peak behavior which leads to the macro-rupture (shaded area) and stage 4, to the shearing along the macro-rupture surface.

Type of Material	σ_c MPa	m
Sidobre granite	165	22
Darley Dale sandstone	70	10
Carrara marble	100	10

Table 1. Parameters of the Hoek and Brown criterion used for the brittle-ductile simulations.

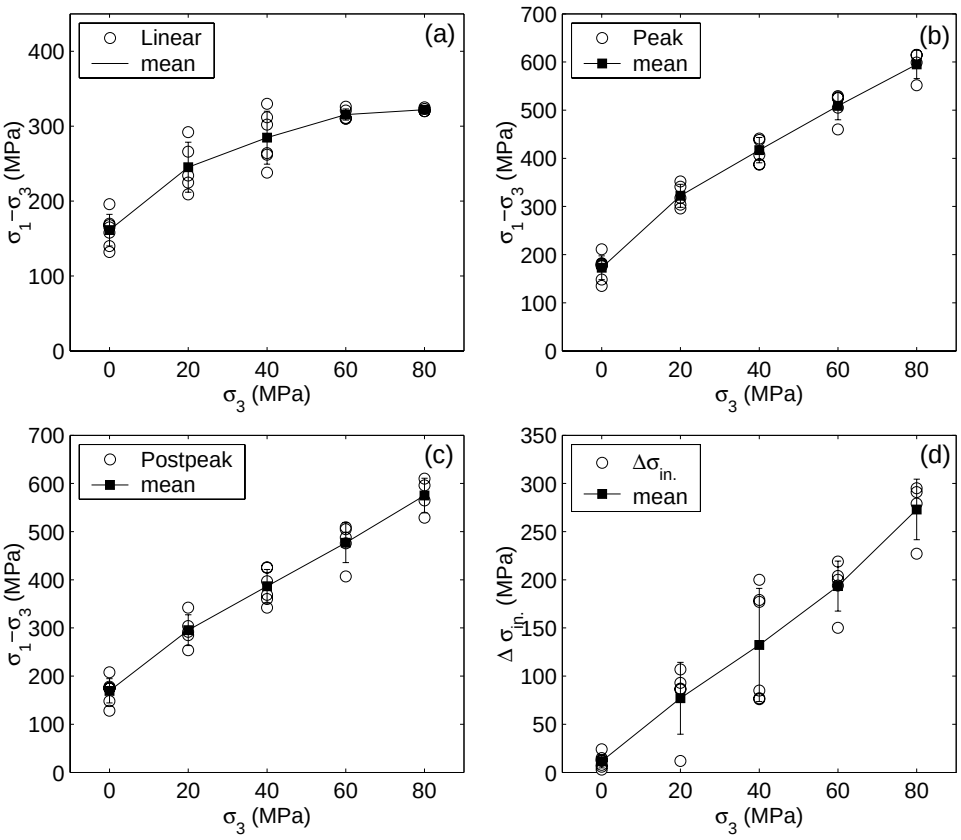

Figure 3. Stress level at the end of the linear stage (a), at the stress peak (b), at the end of the post peak (c), and $\Delta\sigma_{in.}$ (d). $\sigma_1 - \sigma_3$ is plotted as a function of the confining pressure. Open circles correspond to individual values. Black squares correspond to the mean values calculated for each value of confining pressure. Vertical error bars indicate the standard deviation.

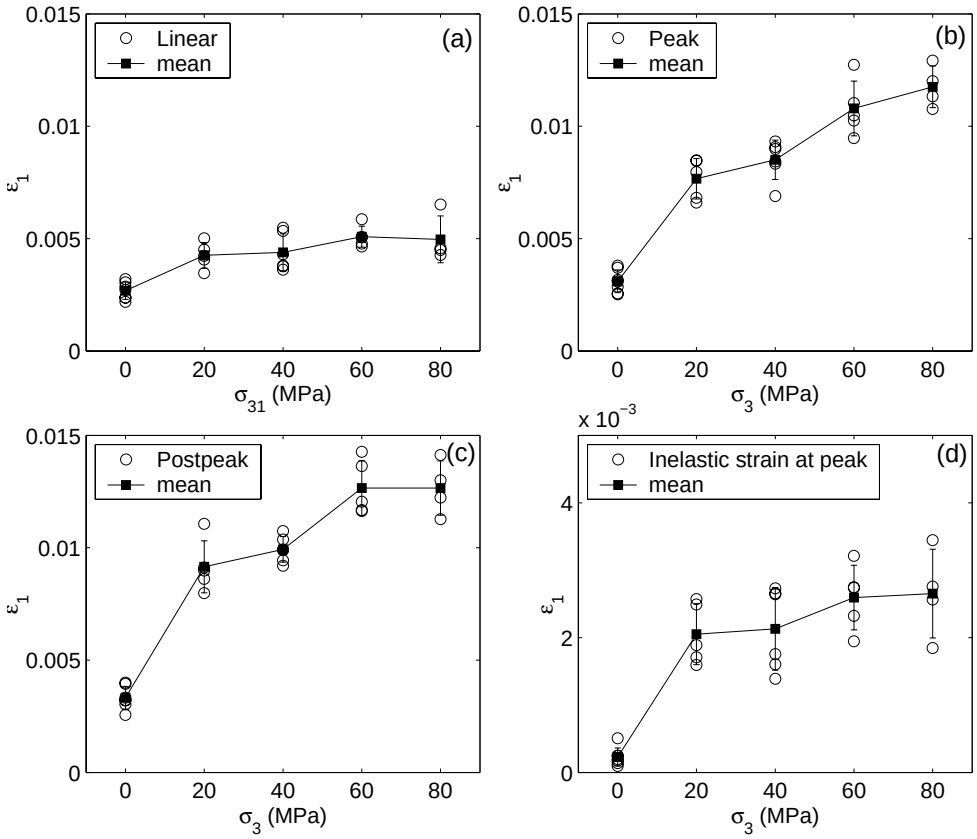

Figure 4. Axial strain at the end of the linear stage (a), at the stress peak (b), at the end of the post-peak stage (c) and inelastic strain at peak (d). Values are plotted as functions of the confining pressure. Open circles correspond to individual values. Black squares correspond the mean values calculated for each value of confining pressure. Vertical error bars indicate the standard deviation.

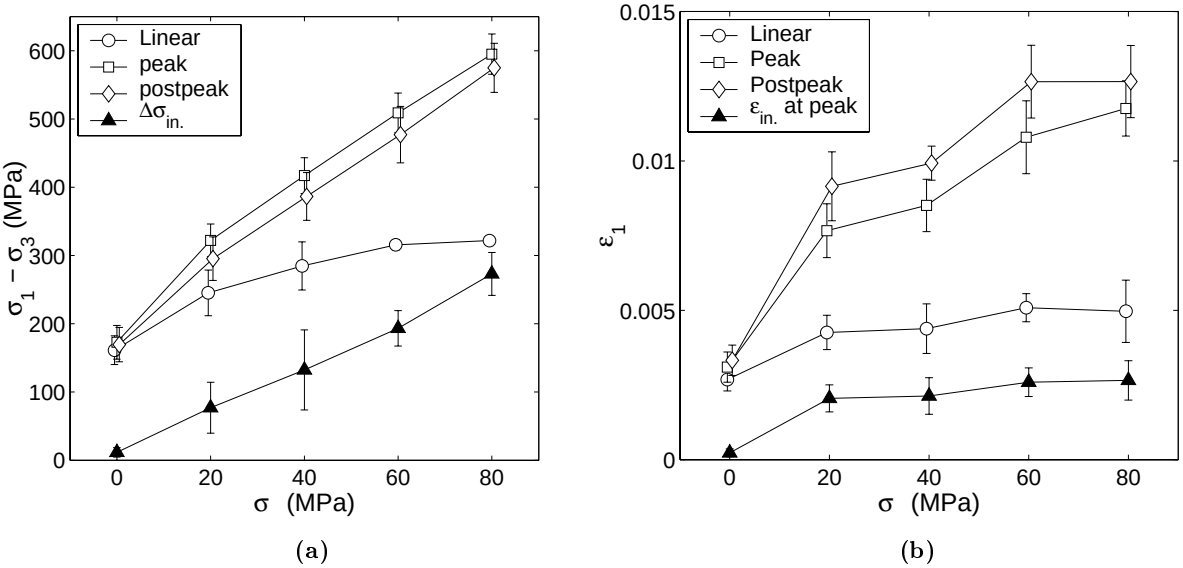

Figure 5. Mean value of the stress (a) and strain (b) for the different stages of the mechanical behavior and $\Delta\sigma_{in.}$ and $\epsilon_{in.}$ as a function of the confining pressure. Vertical error bars indicate the standard deviation.

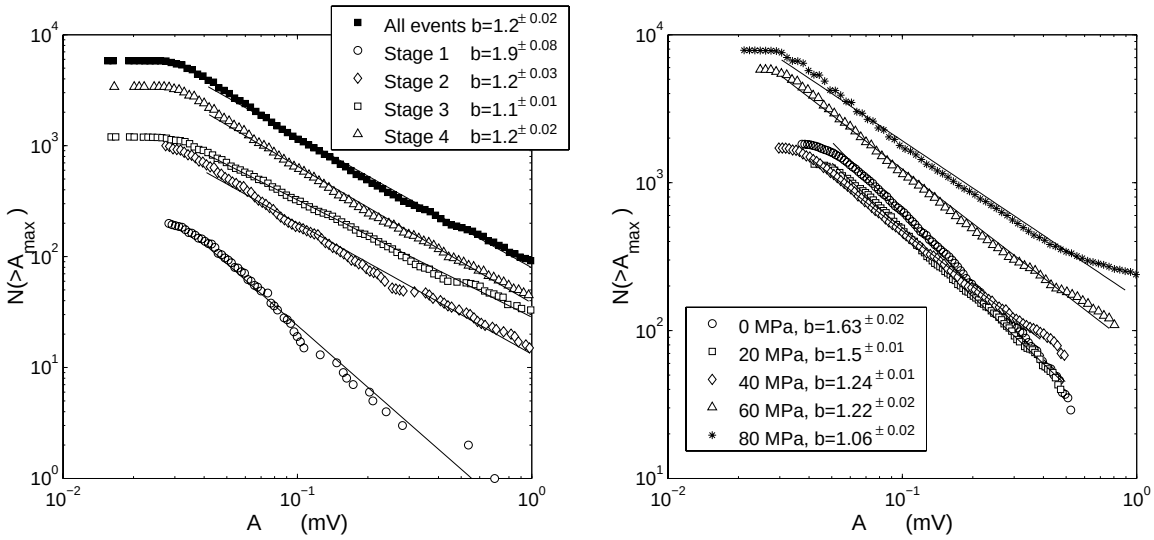

Figure 6. Amplitude distribution of AE event and estimated b-value. a) For the different states of mechanical behavior observed during a single triaxial compression test performed at σ_3=60 MPa. b) For a set of tests performed at different values of confining pressures, each distribution included all the events recorded during each test. The b-values are given with an estimation error for a 95 % confidence level.

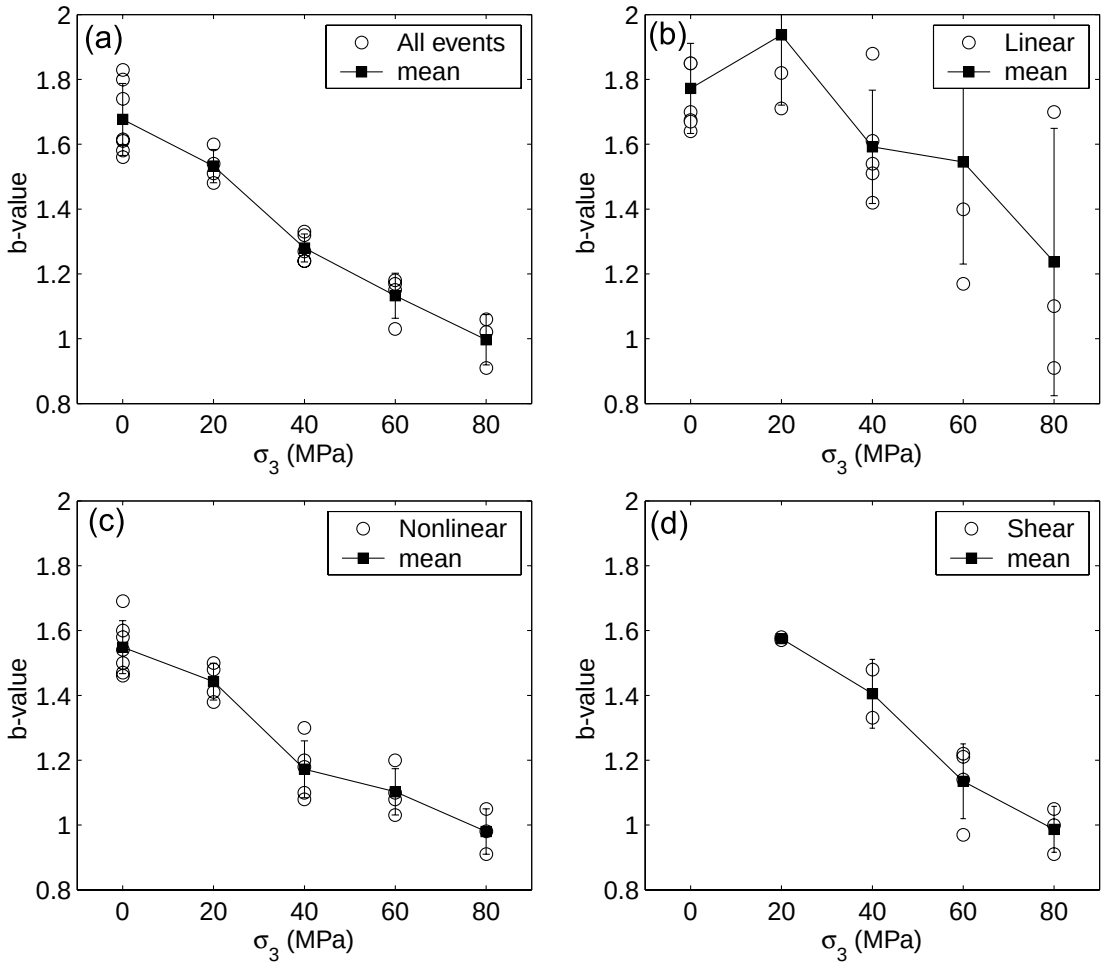

Figure 7. b-value calculated for all AE events recorded during the entire test (a) or for events recorded during each different stage of the mechanical behavior (b-d). The b-value is given with an estimation error for a 95 % confidence level.

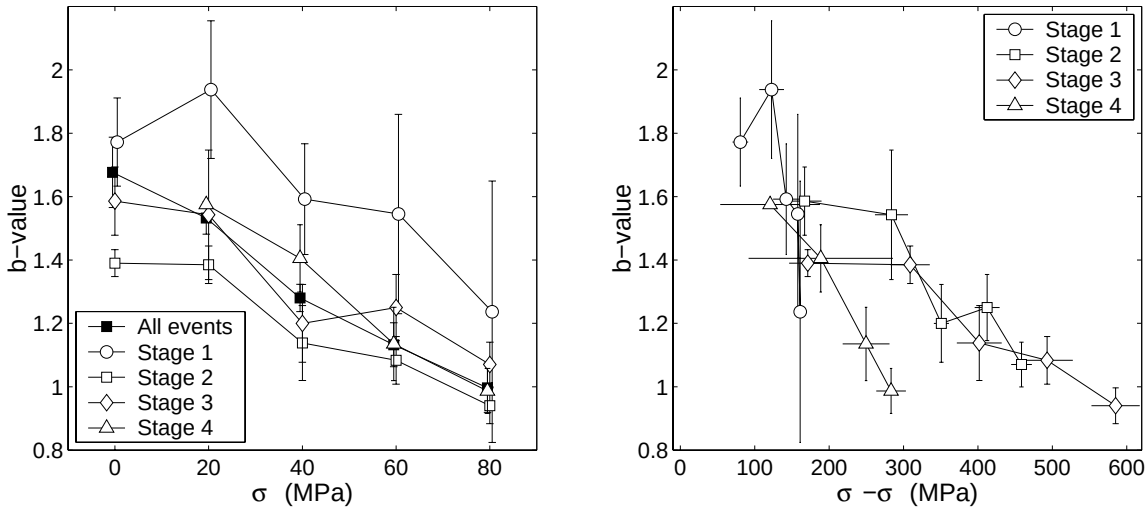

(a) **(b)**

Figure 8. Mean b-value calculated for AE events recorded during the different stages of the mechanical behavior. a) as a function of the confining pressure; b) as a function of the differencial stress $\sigma_1 - \sigma_3$. Horizontal and vertical bars give the standard deviation.

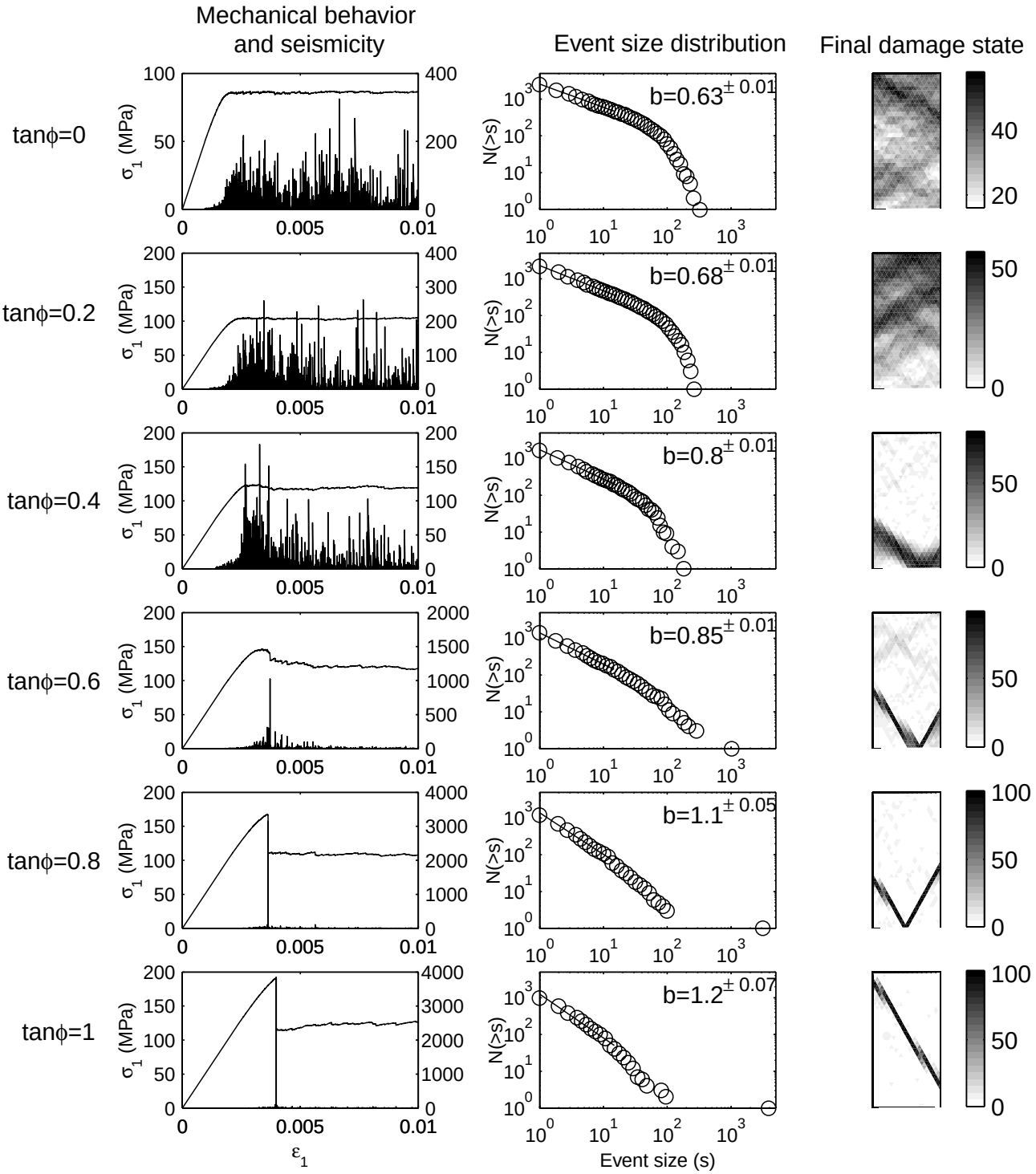

Figure 9. Simulation results performed using the Mohr-Coulomb criterion. Parameters: E=50 GPa, ν=0.25, D=0.05, C: randomly drawn between 25 and 50 MPa, $tan\phi$ ranging from 0 to 1.

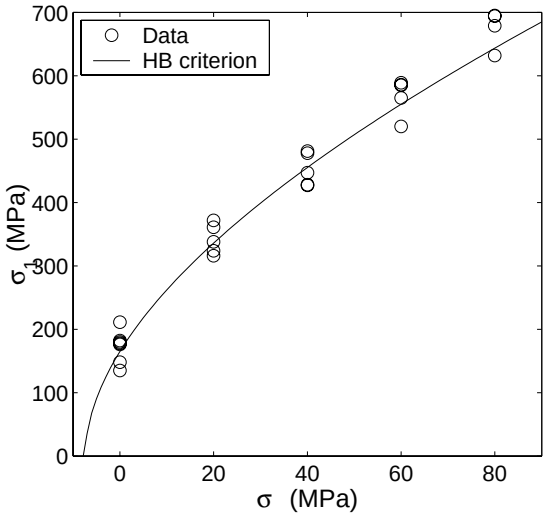

Figure 10. σ_1 at the peak as a function of the confining pressure σ_3 for all the performed test (open circles) and the corresponding Hoek and Brown criterion (σ_c=165 MPa and m=22).

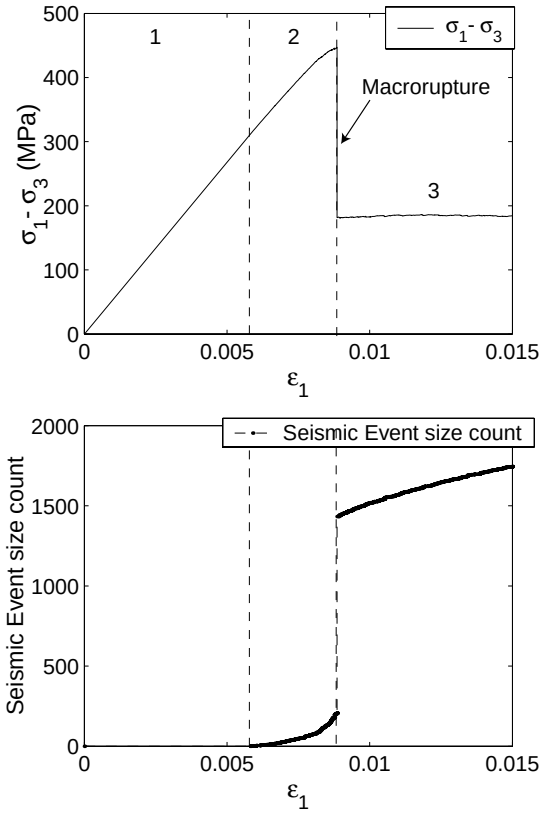

Figure 11. Results obtained from a simulation performed at σ_3=60 MPa. Differential stress, $\sigma_1 - \sigma_3$, and seismic event size count are plotted as a function of longitudinal strain, ϵ_1. Stage 1 corresponds to the linear behavior without seismic activity. Stage 2 corresponds to the onset of seismicity and of non-linear behavior which leads to the macrorupture. Stage 3 corresponds to fault shearing.

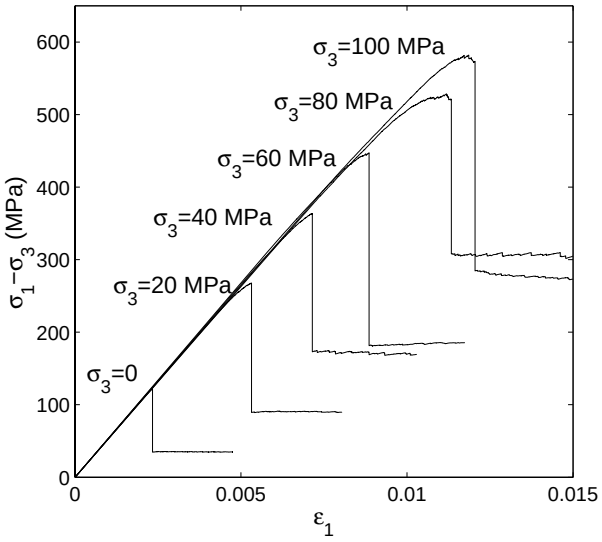

Figure 12. Mechanical behavior observed for simulations of the granite performed at confining pressure values ranging from 0 to 100 MPa.

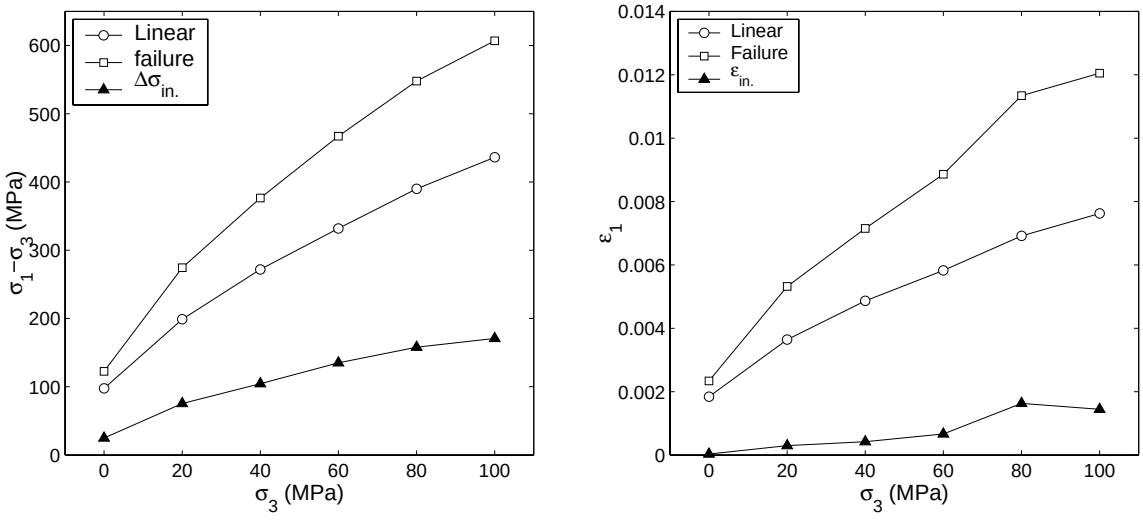

(a) (b)

Figure 13. Stress and strain levels obtained from simulations for different mechanical behaviors stages and $\Delta\sigma_{in.}$ and $\Delta\epsilon_{in.}$ as a function of the confining pressure.

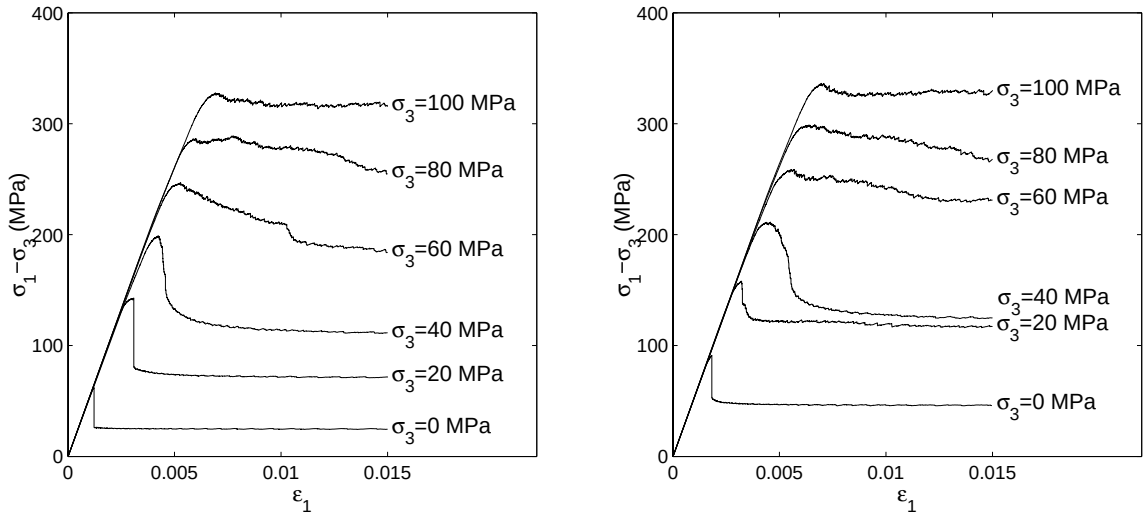

Figure 14. Simulation of the brittle-ductile transition for the Darley-Dale sandstone (a) and the Carrare marble (b).

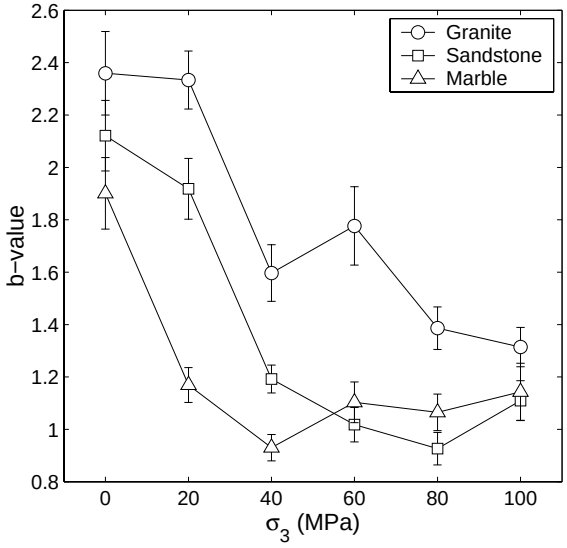

Figure 15. b-value as a function of confining pressure resulting from simulations of the brittle-ductile transition for granite, sandstone and marble.

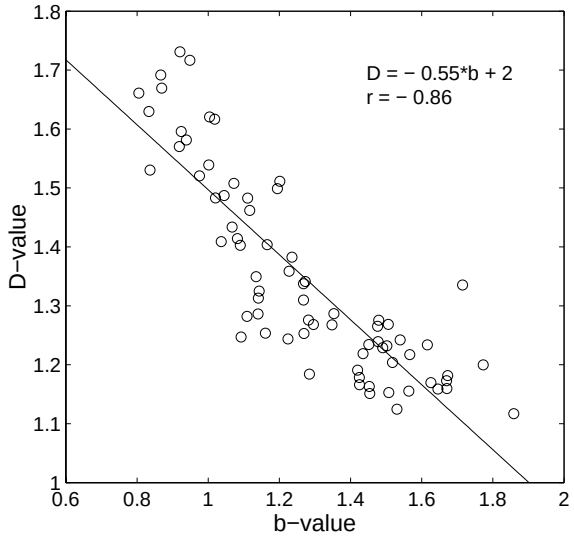

Figure 16. D-value as a function of b-value for 75 simulations performed with various values of σ_c and m parameters. D and b appear to be negatively correlated.